THE JOURNAL OF BIOLOGICAL CHEMISTRY
Vol. 278, No. 31, Issue of August 1, pp. 29072–29078, 2003
Printed in U.S.A.

Functional Implications from an Unexpected Position of the 49-kDa Subunit of NADH:Ubiquinone Oxidoreductase*[S]

Received for publication, March 17, 2003, and in revised form, May 14, 2003
Published, JBC Papers in Press, May 16, 2003, DOI 10.1074/jbc.M302713200

Volker Zickermann‡, Mihnea Bostina§, Carola Hunte¶, Teresa Ruiz§‖, Michael Radermacher§‖, and Ulrich Brandt‡

From the ‡Universität Frankfurt, Fachbereich Medizin, Institut für Biochemie I, D-60590 Frankfurt am Main, Germany, the §Max-Planck-Institut für Biophysik, Abteilung Strukturbiologie, D-60528 Frankfurt am Main, Germany, and the ¶Max-Planck-Institut für Biophysik, Abteilung Membranbiochemie, D-60528 Frankfurt am Main, Germany

Membrane-bound complex I (NADH:ubiquinone oxidoreductase) of the respiratory chain is considered the main site of mitochondrial radical formation and plays a major role in many mitochondrial pathologies. Structural information is scarce for complex I, and its molecular mechanism is not known. Recently, the 49-kDa subunit has been identified as part of the "catalytic core" conferring ubiquinone reduction by complex I. We found that the position of the 49-kDa subunit is clearly separated from the membrane part of complex I, suggesting an indirect mechanism of proton translocation. This contradicts all hypothetical mechanisms discussed in the field that link proton translocation directly to redox events and suggests an indirect mechanism of proton pumping by redox-driven conformational energy transfer.

Complex I (NADH:ubiquinone oxidoreductase)[1] is the major entry point for electrons into the respiratory chain. By linking redox chemistry to vectorial proton translocation, complex I converts up to 40% of the energy used in mitochondria to make ATP. The molecular mechanism of catalysis and its structural basis is not at all understood. Complex I from bovine heart mitochondria is composed of more than 40 different subunits adding to a molecular mass of almost 1000 kDa (1). The enzyme from the strictly aerobic yeast *Yarrowia lipolytica* is of similar size and has been established as a model system to study eucaryotic complex I employing yeast genetics (2, 3). A major obstacle to progress in understanding this extremely large and complicated enzyme complex has been the lack of detailed structural information. Resolutions in the 20–30 Å range have been obtained by electron microscopy of single particles from different organisms that show an L-shaped structure with a hydrophobic arm residing in the membrane and a peripheral arm protruding into the mitochondrial matrix space (2, 4–6). Recently, projection maps from two-dimensional crystals of the bovine enzyme have been obtained at 13 Å resolution (7). Böttcher *et al.* (8) have reported that the enzyme from *Escherichia coli* may change from an L shape to a horseshoe-like shape at zero ionic strength.

The minimal form of the enzyme consists of 14 subunits that are found in both bacterial and mitochondrial complex I (9). In higher eucaryotes seven highly hydrophobic polypeptides are encoded by the mitochondrial genome. All redox prosthetic groups that have been identified so far (eight iron-sulfur clusters and one FMN) are associated with a total of seven hydrophilic and nuclear-coded polypeptides. This poses the problem of how the redox chemistry taking place in the peripheral arm can drive proton translocation across the membrane arm. Evidence from different laboratories (10, 11) and the identification of several pathogenic mutations (12) suggested a key mechanistic role for the 49-kDa, PSST, and TYKY subunits. Based on these indications and a well established homology (13) between the 49-kDa and PSST subunits of complex I and the large and small subunits of [NiFe] hydrogenases, we proposed that at least part of the ubiquinone binding pocket and possibly the proton translocation machinery of complex I have evolved from the domains surrounding the [NiFe] site of the hydrogenase (14). This catalytic core hypothesis was substantiated experimentally by a series of site-directed mutations in the 49-kDa subunit of complex I from *Y. lipolytica* (3). The same studies also provided further support for the previously demonstrated ligation of iron-sulfur cluster N2 by subunit PSST (15, 16), placing this redox center at the interface between the 49-kDa and PSST subunits close to the former [NiFe] binding domain. For further progress in understanding the function of complex I it is essential to localize these key subunits within the structure of this very large membrane protein complex.

EXPERIMENTAL PROCEDURES

Monoclonal Antibodies—A female BALB/c mouse (Harlan/Winkelmann, Borchen, Germany) was immunized by intraperitoneal injection of complex I from *Y. lipolytica* using a long-term protocol. The initial immunization with 100 μl of protein suspension (100 μg of purified protein in 20% (v/v) Gerbu Adjuvant MM, Gerbu Biotechnik GmbH, Gaiberg, Germany) was followed by five injections of 50 μl of protein suspension (50 μg of protein in 20% of the same adjuvant) in 4-week intervals. The final injection was repeated the following day, and the mouse was sacrificed after 2 days for removal of the spleen. The subsequent cell fusion and cell culture work was done according to standard protocols (17). A specific immune response was detected in the serum up to a 10^5-fold dilution, and 4800 clones were obtained from 50% of the cells after cell fusion. The clones were tested by a standard ELISA procedure. For the approach presented here, it was critical to identify antibodies that recognized the native enzyme. Therefore, a His-tag-based ELISA (17) was established to avoid denaturing complex I upon

* This work was supported by the Deutsche Forschungsgemeinschaft (SFB 472), the Fonds der Chemischen Industrie, and Aventis Crop Science. The costs of publication of this article were defrayed in part by the payment of page charges. This article must therefore be hereby marked "*advertisement*" in accordance with 18 U.S.C. Section 1734 solely to indicate this fact.

[S] The on-line version of this article (available at *http://www.jbc.org*) contains supplemental alignments.

‖ Present address: Dept. of Molecular Physiology and Biophysics, College of Medicine, University of Vermont, Burlington, VT 05405.

** To whom correspondence should be addressed: Universität Frankfurt, Fachbereich Medizin, Institut für Biochemie I, Theodor-Stern-Kai 7, Haus 25 B, D-60590 Frankfurt am Main, Germany. Tel.: 49-69-6301-6926; Fax: 49-69-6301-6970; E-mail: brandt@zbc.kgu.de.

[1] The abbreviations used are: complex I, NADH:ubiquinone oxidoreductase; ELISA, enzyme-linked immunosorbent assay; PBS, phosphate-buffered saline; TXPBS, Triton X-100 PBS.

binding to the plates under alkaline conditions and in the absence of detergent. In this native ELISA protocol, the antigen was bound to a nickel-nitrilotriacetic acid-coated support via its hexahistidine sequence (18). All incubation and washing steps were done under mild conditions in the presence of detergent: His-tagged complex I was diluted to 15 μg/ml in coating buffer (50 mM potassium phosphate, pH 7.5, 300 mM NaCl, 0.1% laurylmaltoside) applied to Ni^{2+}-NTA-coated ELISA plates (Qiagen) and incubated for 1 h at room temperature under gentle shaking. After washing (4 cycles, 20 s each) with 20 mM Tris/Cl, pH 7.5, 300 mM NaCl, 0.03% laurylmaltoside 0.2% bovine serum albumin, the cell culture supernatant was adjusted to 50 mM Tris/Cl, pH 8.0, 0.03% laurylmaltoside and incubated for 1 h as above. After washing, a secondary antibody (anti-mouse IgG conjugated to alkaline phosphatase; Sigma) was used for detection of bound antibodies as described in Ref. 17.

About half of the cell lines that gave strong signals after single cell cloning turned out to be of the IgM subtype; others were mainly IgG1. The majority of cell culture supernatants was Western blot-positive, and no cross reactivity with bovine complex I could be observed. Antibodies were purified from cell culture supernatants by hydrophobic charge induction and ion exchange chromatography; the supernatant was applied to an MEP Hypercell column (Kronlab) equilibrated with 50 mM Tris/Cl, pH 8.0. After washing with pure water and 50 mM Tris/Cl, pH 8.0, 25 mM sodium-caprylate, the antibody was eluted with 50 mM sodium-acetate, pH 4.5. Antibody containing fractions were applied to an S-Hyper D column (Biosepra) equilibrated with 50 mM sodium-acetate, pH 4.5, and eluted by changing conditions in a linear gradient to 150 mM NaCl, 50 mM Tris/Cl, pH 7.5.

Epitope Mapping of the 49-kDa Subunit—Synthesis of 218 overlapping decapeptides frameshifted by 2 amino acids was carried out on a cellulose membrane (Abimed) with an ASP222 robot (Abimed) as described in Ref. 19. After complete deprotection the membrane was incubated for 30 min in PBS (100 mM sodium phosphate, pH 7.5, 100 mM NaCl) containing 0.5% Triton X-100 washed with PBS containing 0.1% Triton X-100 (TXPBS) and incubated for several hours to overnight with 5 μg/ml purified antibody in TXPBS. After washing with TXPBS an anti-mouse antibody conjugated to peroxidase (Sigma) was added at a dilution of 1:10000 in TXPBS and incubated for 1 h. Bound antibody was detected by chemoluminescence (ECL system, Amersham Biosciences). For reprobing the membrane with other antibodies, the membrane was washed with 8 M urea, 1% SDS in PBS at room temperature (two times, 30 min) and at 50 °C (1 h), followed by 10% acetic acid, 50% ethanol, 40% water (two times, 10 min). After washing with methanol (two times, 10 min), the membrane was either dried and stored at −20 °C or reprobed starting with the blocking step.

Purification of Complex I from Y. lipolytica and Decoration with Antibodies—Mitochondrial membranes were isolated essentially as described previously (18). However, cells were broken by a glass bead mill operating under continuous flow of material and efficient cooling (Bernd Euler Biotechnology, Frankfurt, Germany). Up to 400 g of cells were processed for 2 h in one liter of 600 mM sucrose, 20 mM Na/Mops, pH 7.0, 1 mM EDTA, 2 mM phenylmethylsulfonyl fluoride. Complex I was purified via His-tag affinity chromatography as described earlier (18) from a *Y. lipolytica* strain containing a chromosomal copy of the NUGM gene carrying a carboxyl-terminal extension coding for a six-alanine and six-histidine tag (3). Complex I was reactivated at a concentration of 1 mg/ml by incubation with an equal volume of 1 mg/ml polar lipids (Avanti) solubilized with 1.6% octyl glucoside. NADH:decylubioquinone activity was measured as described in Ref. 20.

Complex I antibody complexes were prepared by addition of a 2-fold molar excess of antibody to 220 μl of purified complex I at 2 mg/ml. In control samples, the same volume of buffer without antibody was added. The mixture was kept on ice for 30 min. To check for the formation of antigen-antibody complexes, the samples were applied to a TSK 4000 FPLC gel filtration column (Toso-Haas), and the retention time was compared with a chromatogram of complex I without antibody.

Electron Microscopy—For preparing grids, complex I with or without bound antibody was diluted to 0.06 mg/ml, and 6 μl were applied to 400-mesh copper grid coated with a thin carbon film. The specimen was stained with 2% ammonium molybdate using a deep stain technique (21, 22). Micrographs were recorded under low dose condition on a Philips CM120 electron microscope (FEI) equipped with a LaB6 cathode at an accelerating voltage of 100 kV and a calibrated magnification of ×58300. The micrographs were recorded at a defocus of ~1.0 μm. Selected micrographs were scanned on a Zeiss SCAI flat bed scanner (Zeiss) with 7-μm raster size. Images were converted to spider format and reduced three times by binning to a final pixel size of 3.6 Å on the scale of the sample. Particles were interactively selected and windowed into 128 × 128 pixel images. All particles, except obvious small fragments, were selected from micrographs of complex I without antibody. In the case of complex I decorated with antibodies only clear L-shaped particles with an antibody visibly attached were selected.

Image processing was carried out using SPIDER (version 5.0; modified) and WEB (23). All alignments were performed using a simultaneous translational/rotational alignment algorithm, based on correlation of Radon transforms (22). The average image of unlabelled complex I was calculated from a data set of 6000 images. A first alignment was carried out using 900 images and one L-shaped particle as reference. The first alignment result was analyzed using the neural network technique (24), and two nodes were selected representing the "flip" (left-handed) and "flop" (right-handed) L-shaped views. The two node images were used for multireference alignment, again followed by neural network analysis. Four node images were selected from this second analysis and used as starting references for multireference alignment of the full data set (6000 images). The multireference alignment was iterated, recalculating the reference images after each step by averaging the corresponding aligned particle images, which resulted in four class averages. Correspondence analysis (26, 27), combined with Diday's classification by moving centers (28) was applied separately to the four classes. Incomplete particles were excluded. After this process the two major classes (one for the flip orientation, the other for the flop orientation) contained ~1300 particles each.

The contrast transfer function was determined for each micrograph, and every single image was corrected by phase flipping. Each data set was split into two halves, and the corresponding averages were compared by Fourier ring correlation (25). A cutoff value of five times the noise correlation was used as resolution criterion.

The images of complex I labeled with antibodies were aligned in a multireference alignment procedure using the two averages obtained for the native complex I as references. All aligned particles were visually inspected; only those that were well aligned and exhibited a high similarity with the reference were chosen for the final average. For assessment of the significance of the differences, Student's t test was applied.

RESULTS

His-tag-purified complex I was analyzed as single particles in deep negative stain (ammonium molybdate) by electron microscopy. The micrographs (Fig. 1*A*) showed a homogenous distribution of particles and very little aggregation. The angle between the membrane and peripheral arm was found to be variable to a certain extent, ranging from 90° to 150°. For analysis of the heterogeneity of the data set we used a combination of multivariate statistical analysis tools. Self-organizing maps from a neural network algorithm (24) were chosen for a first classification of the data set into four classes differentiated by the orientation relative to the specimen plane and by the angle between the two arms. After multireference alignment correspondence analysis and classification, two major classes containing complete particles were retained totaling 2600 particles and representing ~63% of the image set. The angle between the two arms was 90°, and the particles were almost equally distributed into two classes. They were interpreted as flip view (Fig. 1*B*, *left-handed L*) and the mirrored flop view (Fig. 1*C*, *right-handed L*). Both views are from the side of the supporting carbon on the specimen grid. About the same number of particles were used to calculate two-dimensional averages for the flip and flop views. The resolution was estimated using the Fourier ring correlation with a cutoff value of five times noise correlation. For both averages the resolution was determined to be 25 Å (Fig. 2). Despite the careful classification, the resolution of the two-dimensional averages was limited, most probably because of a residual angular variation and deviations from perfect horizontality of the particles on the grid. The two-dimensional averages were in good agreement with those obtained earlier with complex I from *Y. lipolytica* purified by conventional chromatographic steps (2) and resembled those reported for complex I from bovine heart, *Neurospora crassa*, and *E. coli* (4, 5, 7). An unambiguous assignment of the two perpendicular arms of complex I to a membrane and

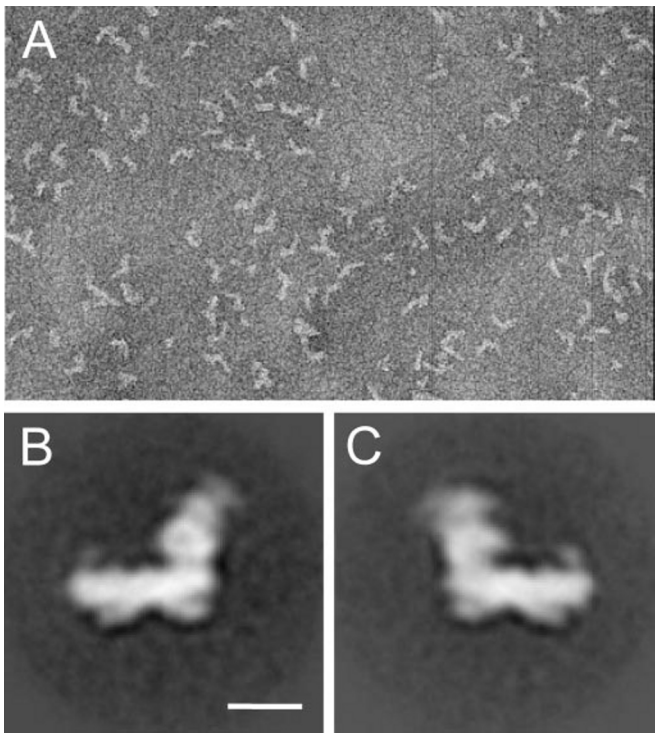

FIG. 1. **Electron microscopy of complex I from *Y. lipolytica.*** *A*, typical micrograph of single particles in negative stain. Flip (left-handed L) (*B*) and flop (right-handed L) (*C*) views of complexes I. The two-dimensional averages were calculated from 1300 particles for each view and represent the two major classes in which the angle between the two arms was 90°. The *scale bar* in panel B represents 100 Å.

a peripheral arm, respectively, had been made for *N. crassa* complex I by comparison of single particles of whole complex I and purified membrane arm (4). The very high structural similarity of the two fungal complexes allowed application of this assignment to the *Y. lipolytica* two-dimensional averages: the peripheral arm of complex I particles from both organisms can be identified most easily by a characteristic protrusion on its inner side (Ref. 4, Fig. 1*C*). Based on this assignment, the membrane arm was oriented horizontally in Fig. 1 of this study and all following figures showing two-dimensional averages of complex I.

In the flop view (Fig. 1*C*) we noted a novel feature, namely a thin bridge-like structure reaching from a protrusion of the peripheral arm to the distal end of the membrane arm. Further studies are under way to investigate the significance of this observation.

From a combined conventional and His-tag-based ELISA screen (17) of 4800 clones from mice immunized with native complex I, 38 clones were found to produce antibodies binding to *Y. lipolytica* complex I. Four of these clones (35C5, 37F3, 42A10, and 34C10) produced IgG-type antibodies against the 49-kDa subunit. In a Western blot all antibodies recognized the 49-kDa subunit and no cross-reactivity with other subunits was observed (not shown). The epitopes of the antibodies were identified by testing their binding to overlapping decapeptides of the 49-kDa subunit sequence. Peptide arrays made by spot synthesis were probed with the individual antibodies. Fig. 3*A* shows the labeling of the two epitopes identified in the 49-kDa subunit: antibodies from three clones (35C5, 37F3, 42A10) recognized the same epitope (designated 49.1) close to the amino terminus, whereas the antibodies from clone 34C10 bound to an epitope (designated 49.2) 55 amino acids downstream of epitope 49.1. Antibody 49.1 from clone 42A10 and antibody 49.2 from clone 34C10 (both subclass IgG1) were used for further analysis. None of the antibodies affected NADH: decylubiquinone oxidoreductase activity of purified complex I that had been reactivated by the addition of phospholipids (20) (data not shown).

The sequence homology between the 49-kDa subunit of complex I and the large subunit from *Desulfovibrio fructosovorans* [NiFe] hydrogenase is low but significant. Several characteristic sequence patterns, *e.g.* the essentially invariant RG*X*E motif (see Fig. 3*B*), are found in virtually all known sequences from both enzyme families (see also alignments in supplemental data). The membrane-bound hydrogenase from *Methanosarcina barkeri* can be considered an evolutionary link to complex I because it still contains a [NiFe] site but shows a much higher degree of homology to complex I, allowing an unambiguous alignment of the subunits from two rather distant families of enzymes. Sequence alignment of the amino-terminal part of the 49-kDa sequence from different organisms and the large subunit of two different [NiFe] hydrogenases revealed that the portion of the protein around epitope 49.1 is missing in the bacterial homologues of the 49-kDa subunit and that it has no similarity to the corresponding sequence of the large hydrogenase subunit. The sequence around epitope 49.2 of *Y. lipolytica* complex I exhibited a high degree of homology between 49-kDa subunits of different origin and could be aligned to the corresponding part of the hydrogenase subunit (Fig. 3*B*). Notably, the decapeptide identified as epitope 49.2 matched the middle strand of a three-stranded β-sheet on the surface of the protein in the known structure of *D. fructosovorans* [NiFe] hydrogenase (Fig. 3*C*). The cascaded multiple classifiers algorithm for secondary structure prediction (29) predicted three matching β-strands in this part of mitochondrial and bacterial 49-kDa subunits (Fig. 3*B*), strongly suggesting that, as shown previously for the fold around the [NiFe] site (3), the β-sheet and the overall structure around epitope 49.2 has been preserved in complex I.

In *E. coli* there is a direct fusion of the carboxyl terminus of the 30-kDa subunit of complex I to the amino terminus of the 49-kDa subunit forming the NuoCD protein (9). The homology of the NuoCD subunit to individual subunits from other organisms is high, and there are no insertions. It follows for the structure of complex I from *Y. lipolytica* that the carboxyl-terminal end of the 30-kDa subunit is expected to reside in the vicinity of the amino-terminal epitope 49.2. To test this prediction, we included a commercially available anti-His-tag antibody in this study to locate the His-tag sequence that had been attached to the carboxyl terminus of the 30-kDa subunit to purify complex I from *Y. lipolytica* (18).

The antibody-complex I complexes used for electron microscopy were prepared by incubating a 2-fold excess of antibody with purified complex I. Formation of stable complexes with the native enzyme was confirmed for all antibodies used in this study as clear shifts of retention time in analytical gel filtration in comparison to complex I alone (data not shown). Gel filtration was also used in some experiments to remove excess antibody before preparing the grids for electron microscopy, without any detectable effect on the results (not shown).

About 10–25% of complex I particles were found by visual inspection of the micrographs (Fig. 4) to be labeled with an antibody. Only those particles were aligned and averaged that exhibited a high similarity with the 90° flip or flop reference (Fig 5, *A–D*). For antibody 49.2 a 40:60 distribution of flip and flop views of decorated complex I was observed. The vast majority of particles was in flip view orientation when labeled with antibody 49.1 and in flop view orientation when labeled with the His-tag antibody. All three antibodies against hydrophilic subunits of complex I were found to bind to the part of the

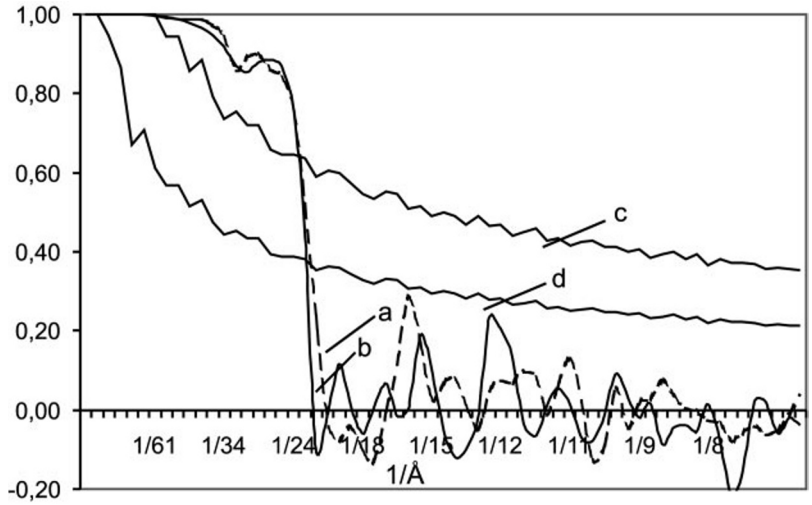

FIG. 2. **Resolution of unlabelled complex I averages.** Fourier ring correlation curves of averages shown in Fig. 1, flip (*a*) and flop (*b*) positions. The resolution was 25 Å using the five times noise correlation criterion, curve (*c*) and 21 Å using the three times noise correlation criterion, curve (*d*).

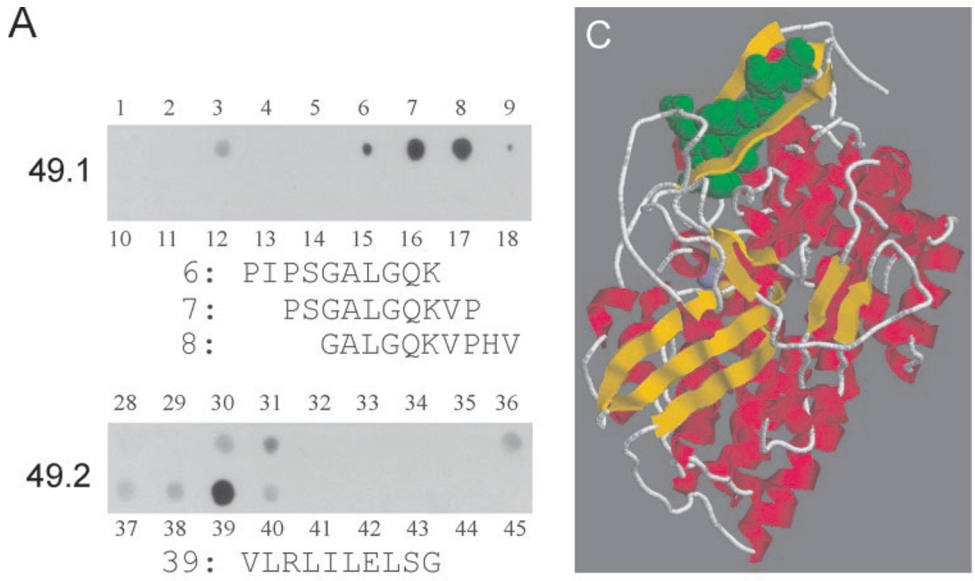

FIG. 3. **Epitope mapping and structure prediction of the 49-kDa subunit.** *A*, identification of two different epitopes with monoclonal antibodies recognizing the 49-kDa subunit. Three cellulose membranes with 218 overlapping decapeptides covering the sequence of the *Y. lipolytica* 49-kDa subunit were probed with antibodies 42A10 (*49.1*) and 34C10 (*49.2*). Sections of the filters identifying the epitopes are shown. The peptide sequence of spots exhibiting clear antibody binding is given. *B*, alignment of the amino-terminal regions of the 49-kDa subunits of complex I from *Y. lipolytica*, *N. crassa*, and *E. coli* around epitope 49.2 aligned with the amino-terminal part of the EchE subunit from the membrane-bound [NiFe] hydrogenase and the large subunit of the soluble [NiFe] hydrogenase from *D. fructosovorans*. *Red*, epitope 49.2; *blue*, invariant RG*X*E motif; *green*, two of the cysteines ligating the [NiFe] site in hydrogenase; *green-shaded*, amino acids forming the amino-terminal β-strands in the structure of the large subunit of hydrogenase; *yellow-shaded*, predicted β-strands in other sequences. *C*, schematic of the structure of the large subunit of [NiFe] hydrogenase from *D. fructosovorans* (PDB number 1FRF) highlighting the β-strand (*green spacefill*) that corresponds to epitope 49.2 in the 49-kDa subunit of complex I. The [NiFe] center (in *purple/yellow spacefill*) resides at a distance of about 30 Å from the most distant residue of the highlighted β-strand.

particles previously identified as peripheral arm, confirming the assignment of these two major parts of the complex I structure.

To better define the contact site between the antibodies and complex I, a Student's *t* test was performed to compare the native with the labeled complex. Images were obtained by averaging previously aligned particles, and the corresponding variance images were calculated. The coincidence of the mean values of each pixel in both images was tested. The pixels for which the confidence level was greater than 95% were set to zero, and only those with a statistical significant difference remained. In Fig. 5, *E–H*, the results are presented together with the contour of the complex I traced at a value corresponding to one-fifth of the variance of the image.

Antibody 49.1 (Fig. 5, *A* and *E*) was seen as an extra mass at the tip of the protrusion of the peripheral arm. The mass of the antibody was rather disordered, and the Student's *t* test showed the most significant differences somewhat distant from

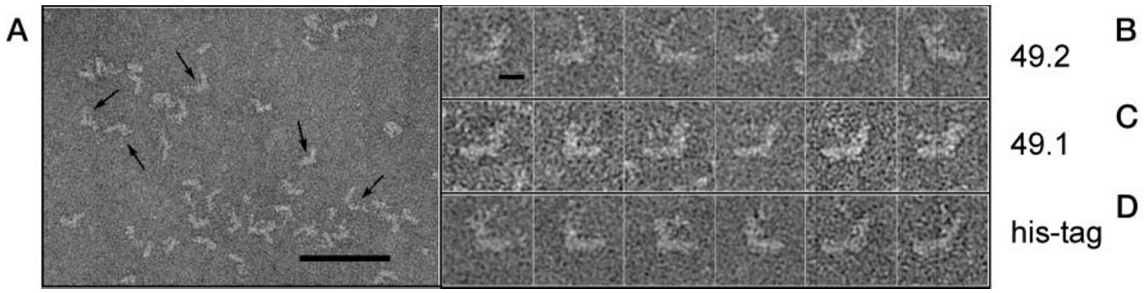

FIG. 4. **Individual complex I particles decorated with antibodies.** *A*, typical micrograph of single particles labeled with antibody 49.2 in negative stain. The *arrows* indicate particles that were identified as clearly binding an antibody and were used for further analysis. *Scale bar*, 0.1 μm. *B–D*, gallery of single particles decorated with antibody 49.1, antibody 49.2, and His-tag antibody, respectively. *Scale bar*, 100 Å.

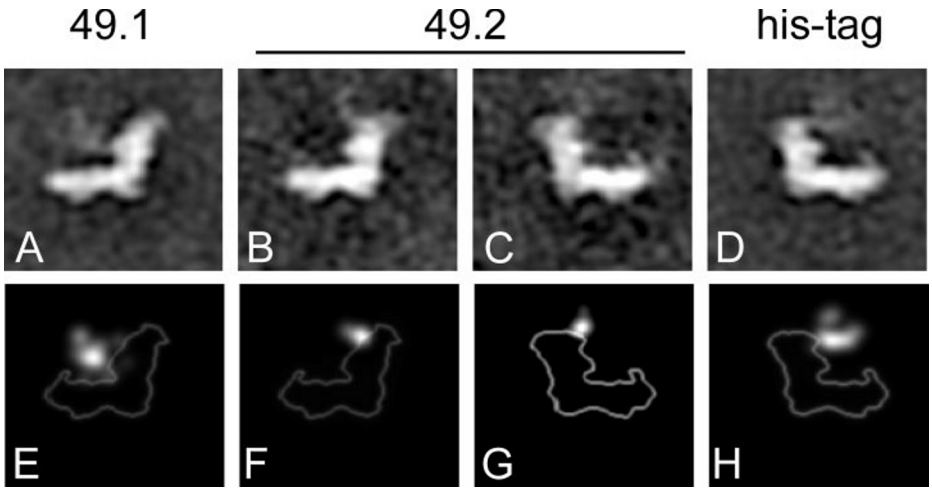

FIG. 5. **Two-dimensional averages of single particles decorated with antibodies.** *A*, average of 60 complex I particles decorated with antibody 49.1 in flip view. *B* and *C*, average of 60 complex I particles decorated with antibody 49.2 in flip (*B*) and flop (*C*) view. *D*, average of 60 complex I particles decorated with anti-His-tag antibody in flop view. Because of a clear preference for either the flip or flop orientation, mirrored averages were not calculated for antibody 49.1 and the anti-His-tag antibody. *E–H*, Student's *t* test of the averages shown in *panels A–D*. *Light areas* indicate a statistical difference between labeled and unlabeled particles (confidence level >95%). The contour lines of the unlabelled averages (Fig. 1) were superimposed over the Student's *t* test images.

the contour of complex I. This may be because of flexibility of the amino terminus of the 49-kDa subunit combined with the inherent flexibility of an antibody molecule (30). In line with the pronounced antigenicity of epitope 49.1, binding of polyclonal Fab fragments to the same region of the 49-kDa subunit of *N. crassa* complex I was reported earlier (31). In bacterial complex I and hydrogenase this part of the corresponding subunits is missing.

Antibody 49.2 bound very rigidly to complex I and was seen in both the flip (Fig. 5, *B* and *F*) and the flop (Fig. 5, *C* and *G*) views as clear extra mass attached to the peripheral arm of complex I. This suggested binding to a more rigid epitope and is consistent with the prediction of a β-strand (Fig. 3*B*) and the structural homology with the large subunit of [NiFe] hydrogenase for this sequence stretch (Fig. 3*C*). The more rigid binding is reflected by a more constrained difference area seen in the Student's *t* test analysis. The position of the binding site in both views was ~50 Å apart from antibody 49.1 and ~100 Å away from the membrane arm. Epitopes 49.1 and 49.2 are separated by 55 amino acids, which is more than sufficient to bridge a distance of ~50 Å.

The His-tag at the carboxyl-terminus of the 30-kDa subunit was localized using a commercially available anti-His-tag antibody. As expected, the binding site of this antibody (Fig. 5, *D* and *H*) was found to be in the vicinity of the 49.2 epitope, somewhat closer to the membrane arm. The constraint for the orientation of the antibody seemed to be intermediate as compared with the other two antibodies. This may be explained by some flexibility of the His-tag itself that had been attached via a six-alanine linker (18). Because epitope 49.1 was found in a position much closer to the membrane arm, it can be concluded that the additional 20–30 amino-terminal amino acids not present in the 49-kDa subunits of bacterial complexes extend the 49-kDa subunit into this direction in eucaryotic complexes.

DISCUSSION

In recent years, several lines of evidence have shown that the 49-kDa subunit plays a central role for the mechanism of complex I. Specific mutations in the 49-kDa were identified, which cause severe cardiomyopathy and encephalopathy in humans (32). Several point mutations near the carboxyl terminus of the 49-kDa subunit were shown to cause resistance toward complex I inhibitors in *Rhodobacter capsulatus* (11, 33) and *Y. lipolytica* (14). Other site-directed mutations in this subunit of *Y. lipolytica* complex I gave rise to specific alterations in the EPR spectra of the functionally critical iron-sulfur cluster N2 and virtually complete loss of ubiquinone reductase activity (14). Based on the homology to the 49-kDa and PSST subunits from complex I (13, 34), the known structure of [NiFe] hydrogenases (35, 36) was established as a guide to understand the structural implications of mutations in complex I. From the effects that were caused by individual mutations in the 49-kDa subunit, it became clear that the fold harboring the [NiFe] cluster of hydrogenase is retained in the 49-kDa subunit as the central part of a catalytic core conferring the ubiquinone reductase function of complex I (3, 37). In addition, the coupling of iron-sulfur cluster N2 with semiquinone radicals (38) further substantiated the idea that proton translocation by complex I is

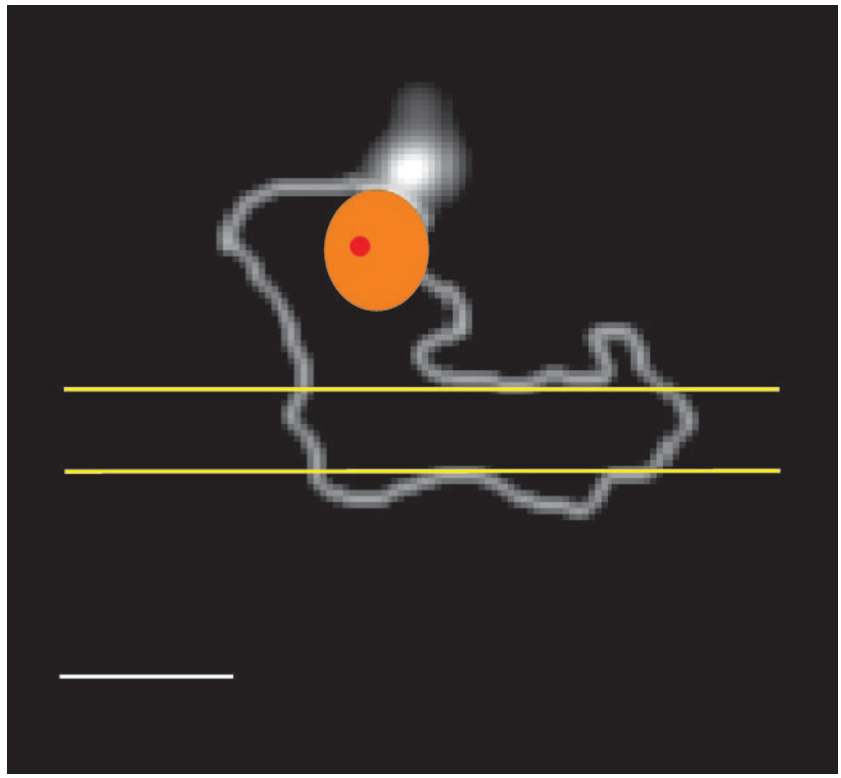

FIG. 6. **Schematic representation of the position of the 49-kDa subunit within a complex I particle.** The approximate position of the 49-kDa subunit is shown as the *orange area* superimposed over the outline of complex I decorated with antibody 49.2 (Fig. 5*G*). The size of the area reflects the dimensions of the large subunit of [NiFe] hydrogenase (35). The *red dot* indicates the approximate position of the [NiFe] site. *Scale bar*, 100 Å. See "Discussion" for further details.

coupled to the redox chemistry of ubiquinone in an integrated pump device consisting of iron-sulfur cluster N2 and the ubiquinone reduction site (37, 39).

In this study we have located two epitopes within the 49-kDa subunit in the electron microscopic structure of complex I. By sequence, the 49-kDa subunit is a hydrophilic subunit without any predicted transmembrane regions. The sequence of the 49.2 epitope is homologous to the second strand of a three-stranded amino-terminal β-sheet in hydrogenase (compare Fig. 3). In line with structure prediction analysis of the amino-terminal part of the 49-kDa subunit, we propose that this fold is conserved in the complex I subunit. Considering the already demonstrated structural conservation of the [Ni-Fe] binding domain in hydrogenase and complex I including the carboxyl terminus of the 49-kDa subunit, it seems justified to conclude that the overall fold of both proteins essentially has been conserved during evolution. Based on these considerations we took the dimensions of the large hydrogenase subunit as an estimate for the size of the 49-kDa subunit. The resulting maximal distance between epitope 49.2 and the opposite end of the subunit is about 70 Å. As illustrated in Fig. 6, this suggests that the minimal distance between the 49-kDa subunit and the membrane arm of complex I is in the order of 30–40 Å, and the domain around the former [NiFe] site is predicted to be as much as 70–80 Å away from the membrane domain. We conclude that the entire 49-kDa subunit is clearly separated from the membrane arm of complex I and that the functionally critical domains will be found in the distal half of the peripheral arm.

There is ample evidence that the catalytic core closely interacts with hydrophobic compounds like ubiquinone and inhibitors. Therefore, our finding that this part of complex I is clearly separated and at a remarkable distance from the membrane arm is quite unexpected and has far-reaching implications for our understanding of the mechanism of this proton pumping respiratory chain enzyme. It should be stressed again at this point that the binding of three different monoclonal antibodies directed against hydrophilic central subunits to the part of complex I previously identified as the peripheral arm in itself is strong proof for the correctness of this assignment.

Recently, Böttcher *et al*. (8) have proposed that in the active conformation of *E. coli* complex I part of the peripheral arm bends over to the membrane arm, resulting in a horse-shoe shaped complex. Apart from the fact that the existence and significance of this conformation is controversially discussed in the field (40), it should be noted also that the proposed horse-shoe conformation of complex I does not resolve the issue discussed here: the authors identified the peripheral part of complex I bending down to the membrane arm in the horse-shoe conformation as the NADH-dehydrogenase domain, while the hydrogenase module of complex I comprising the catalytic core was reported to not move during the proposed conformational change.

The alternative left to reconcile the peripheral location of the catalytic core of complex I and its interaction with ubiquinone and inhibitors is to assume that these hydrophobic compounds leave the membrane domain to reach their binding site above the plane defined by the phospholipid headgroups. Ubiquinone is a hydrophobic molecule, and at first sight it seems rather far-fetched to assume that it should react at a site clearly distant from the membrane part. However, earlier observations are not in conflict with this view, and a rather consistent picture of the ubiquinone reactive domain of complex I can be drawn: the enzyme from bovine heart has been split into subcomplexes, one of which contains only hydrophilic subunits, including the 49-kDa subunit (41). The electron transfer rate of this subcomplex Iλ using the hydrophilic ubiquinone analogue Q1 as a substrate is comparable with that of the complete enzyme but insensitive to the classic complex I inhibitor, rotenone. This was previously interpreted as suggesting an alternate, non-physiological ubiquinone reduction site in the subcomplex. In the light of the findings reported here, however, this ubiquinone binding site in the peripheral portion of complex I may, in fact, represent the hydrophilic part of the physiological ubiquinone binding pocket that is made accessible for hydrophilic compounds like Q1 in the subcomplex. Complex I is

known to react with a large number of chemically very diverse inhibitor compounds and is well known to loose activity and inhibitor sensitivity upon purification. The hydrophobic inhibitors were shown to bind to only one large binding pocket with overlapping binding sites (42), and the purified enzyme can be fully reactivated by the addition of lipids (20). Our results provide a new perspective to understand these rather peculiar features of complex I. We suggest that a hydrophobic ramp or crevice connects the membrane part and the catalytic site in the peripheral arm, providing a route for ubiquinone. This "ramp hypothesis" would imply that many of the hydrophobic inhibitors of complex I may act simply by blocking this route somewhere.

From a conceptual point of view it was discussed that complex I is governed by a ligand conduction mechanism based on the redox chemistry of ubiquinone (39, 44). On a structural basis our results render such a mechanism highly unlikely because as a prerequisite this would require that the redox-linked protonation/deprotonation reaction of ubiquinone was directly associated with the membrane domain. The recent finding that in certain enterobacteria complex I pumps Na^+ instead of H^+ also is difficult to reconcile with any direct type of proton pumping mechanism (45). In conclusion we are left with the option that an indirect mechanism of proton pumping via long-range conformational energy transfer is operating in mitochondrial complex I. Some biochemical evidence in favor of this option has been provided by monitoring redox state-dependent changes in the cross-linking pattern of complex I (43). At this point the most likely scenario is that the redox chemistry of ubiquinone reduction around iron-sulfur cluster N2 induces specific conformational changes. These changes are then transmitted to the hydrophobic subunits in the membrane that act as ion pumps.

Acknowledgments—We thank Stefan Kerscher for performing the structure prediction analysis and Franz Streb and Karin Siegmund for excellent technical assistance.

REFERENCES

1. Walker, J. E. (1992) *Q. Rev. Biophys.* **25,** 253–324
2. Djafarzadeh, R., Kerscher, S., Zwicker, K., Radermacher, M., Lindahl, M., Schägger, H., and Brandt, U. (2000) *Biochim. Biophys. Acta* **1459,** 230–238
3. Kerscher, S., Dröse, S., Zwicker, K., Zickermann, V., and Brandt, U. (2002) *Biochim. Biophys. Acta-Bioenerg.* **1555,** 83–91
4. Hofhaus, G., Weiss, H., and Leonard, K. (1991) *J. Mol. Biol.* **221,** 1027–1043
5. Guenebaut, V., Schlitt, A., Weiss, H., Leonard, K., and Friedrich, T. (1998) *J. Mol. Biol.* **276,** 105–112
6. Grigorieff, N. (1998) *J. Mol. Biol.* **277,** 1033–1046
7. Sazanov, L. A., and Walker, J. E. (2000) *J. Mol. Biol.* **392,** 455–464
8. Böttcher, B., Scheide, D., Hesterberg, M., Nagel-Steger, L., and Friedrich, T. (2002) *J. Biol. Chem.* **277,** 17970–17977
9. Friedrich, T. (1998) *Biochim. Biophys. Acta* **1364,** 134–146
10. Schuler, F., Yano, T., Di Bernardo, S., Yagi, T., Yankovskaya, V., Singer, T. P., and Casida, J. E. (1999) *Proc. Natl. Acad. Sci. U. S. A.* **96,** 4149–4153
11. Darrouzet, E., Issartel, J. P., Lunardi, J., and Dupuis, A. (1998) *FEBS Lett.* **431,** 34–38
12. Smeitink, J., Van den Heuvel, L., and DiMauro, S. (2001) *Nat. Rev. Genet.* **2,** 342–352
13. Böhm, R., Sauter, M., and Böck, A. (1990) *Mol. Microbiol.* **4,** 231–243
14. Kashani-Poor, N., Zwicker, K., Kerscher, S., and Brandt, U. (2001) *J. Biol. Chem.* **276,** 24082–24087
15. Rasmussen, T., Scheide, D., Brors, B., Kintscher, L., Weiss, H., and Friedrich, T. (2001) *Biochemistry* **40,** 6124–6131
16. Duarte, M., Populo, H., Videira, A., Friedrich, T., and Schulte, U. (2002) *Biochem. J.* **364,** 833–839
17. Padan, E., Venturi, M., Michel, H., and Hunte, C. (1998) *FEBS Lett.* **441,** 53–58
18. Kashani-Poor, N., Kerscher, S., Zickermann, V., and Brandt, U. (2001) *Biochim. Biophys. Acta* **1504,** 363–370
19. Venturi, M., Rimon, A., Gerchman, Y., Hunte, C., Padan, E., and Michel, H. (2002) *J. Biol. Chem.* **275,** 4734–4742
20. Dröse, S., Zwicker, K., and Brandt, U. (2002) *Biochim. Biophys. Acta* **1556,** 65–72
21. Stoops, J. K., Kolodziej, S. J., Schroeter, J. P., Bretaudiere, J. P., and Wakil, S. J. (1992) *Proc. Natl. Acad. Sci. U. S. A.* **89,** 6585–6589
22. Radermacher, M., Ruiz, T., Wieczorek, H., and Gruber, G. (2001) *J. Struct. Biol.* **135,** 26–37
23. Frank, J., Radermacher, M., Penzcek, P., Zhu, J., Li, Y., Ladjadj, M., and Leith, A. (1996) *J. Mol. Biol.* **161,** 134–137
24. Marabini, R., Masegosa, I. M., San Martin, M. C., Marco, S., Fernandez, J. J., de la Fraga, L. G., Vaquerizo, C., and Carazo, J. M. (1996) *J. Struct. Biol.* **116,** 237–240
25. Saxton, W. O., and Baumeister, W. (1982) *J. Microsc.* **127,** 127–138
26. Frank, J., and van Heel, M. G. (1982) *J. Mol. Biol.* **161,** 134–137
27. van Heel, M., and Frank, J. (1981) *Ultramicroscopy* **6,** 187–194
28. Diday, E. (1971) *Rev. Stat. Appl.* 19–34
29. Ouali, M., and King, R. D. (2000) *Protein Sci.* **9,** 1162–1176
30. Lesk, A. M., and Chothia, C. (1988) *Nature* **335,** 188–190
31. Guenebaut, V., Vincentelli, R., Mills, D., Weiss, H., and Leonard, K. R. (1997) *J. Mol. Biol.* **265,** 409–418
32. Loeffen, J., Elpeleg, O., Smeitink, J., Smeets, R., Stöckler-Ipsiroglu, S., Mandel, H., Sengers, R., Trijbels, F., and Van den Heuvel, L. (2001) *Ann. Neurol.* **49,** 195–201
33. Prieur, I., Lunardi, J., and Dupuis, A. (2001) *Biochim. Biophys. Acta* **1504,** 173–178
34. Albracht, S. P. J. (1993) *Biochim. Biophys. Acta* **1144,** 221–224
35. Volbeda, A., Charon, M. H., Piras, C., Hatchikian, E. C., Frey, M., and Fontecilla-Camps, J. C. (1995) *Nature* **373,** 580–587
36. Montet, Y., Amara, P., Volbeda, A., Vernede, X., Hatchikian, E. C., Field, M. J., Frey, M., and Fontecilla-Camps, J. C. (1997) *Nature Struct. Biol.* **4,** 523–526
37. Kerscher, S., Kashani-Poor, N., Zwicker, K., Zickermann, V., and Brandt, U. (2001) *J. Bioenerg. Biomembr.* **33,** 187–196
38. Magnitsky, S., Toulokhonova, L., Yano, T., Sled, V. D., Hagerhall, C., Grivennikova, V. G., Burbaev, D. S., Vinogradov, A. D., and Ohnishi, T. (2002) *J. Bioenerg. Biomembr.* **34,** 193–208
39. Brandt, U. (1999) *BioFactors* **9,** 95–101
40. Sazanov, L. A., Carroll, J., Holt, P., Toime, L., and Fearnley, I. M. (2003) *J. Biol. Chem.* **278,** 19483–19489
41. Finel, M., Majander, A. S., Tyynelä, J., de Jong, A. M. P., Albracht, S. P. J., and Wikström, M. K. F. (1994) *Eur. J. Biochem.* **226,** 237–242
42. Okun, J. G., Lümmen, P., and Brandt, U. (1999) *J. Biol. Chem.* **274,** 2625–2630
43. Belogrudov, G., and Hatefi, Y. (1994) *Biochemistry* **33,** 4571–4576
44. Dutton, P. L., Moser, C. C., Sled, V. D., Daldal, F., and Ohnishi, T. (1998) *Biochim. Biophys. Acta* **1364,** 245–257
45. Gemperli, A. C., Dimroth, P., and Steuber, J. (2003) *Proc. Natl. Acad. Sci. U. S. A.* **100,** 839–844